Molecular Cancer Therapeutics

Characterization of ABBV-221, a Tumor-Selective EGFR-Targeting Antibody Drug Conjugate

Andrew C. Phillips[1], Erwin R. Boghaert[1], Kedar S. Vaidya[1], Hugh D. Falls[1], Michael J. Mitten[1], Peter J. DeVries[1], Lorenzo Benatuil[2], Chung-Ming Hsieh[2], Jonathan A. Meulbroek[1], Sanjay C. Panchal[1], Fritz G. Buchanan[1], Kenneth R. Durbin[1], Martin J. Voorbach[1], David R. Reuter[1], Sarah R. Mudd[1], Lise I. Loberg[1], Sherry L. Ralston[1], Diana Cao[3], Hui K. Gan[3], Andrew M. Scott[3], and Edward B. Reilly[1]

Abstract

Depatuxizumab mafodotin (depatux-m, ABT-414) is a tumor-selective antibody drug conjugate (ADC) comprised of the anti-EGFR antibody ABT-806 and the monomethyl auristatin F (MMAF) warhead. Depatux-m has demonstrated promising clinical activity in glioblastoma multiforme (GBM) patients and is currently being evaluated in clinical trials in first-line and recurrent GBM disease settings. Depatux-m responses have been restricted to patients with amplified EGFR, highlighting the need for therapies with activity against tumors with nonamplified EGFR overexpression. In addition, depatux-m dosing has been limited by corneal side effects common to MMAF conjugates. We hypothesized that a monomethyl auristatin E (MMAE) ADC utilizing an EGFR-targeting antibody with increased affinity may have broader utility against tumors with more modest EGFR overexpression while mitigating the risk of corneal side effects. We describe here preclinical characterization of ABBV-221, an EGFR-targeting ADC comprised of an affinity-matured ABT-806 conjugated to MMAE. ABBV-221 binds to a similar EGFR epitope as depatux-m and retains tumor selectivity with increased binding to EGFR-positive tumor cells and greater *in vitro* potency. ABBV-221 displays increased tumor uptake and antitumor activity against wild-type EGFR-positive xenografts with a greatly reduced incidence of corneal side effects relative to depatux-m. ABBV-221 has similar activity as depatux-m against an EGFR-amplified GBM patient derived xenograft (PDX) model and is highly effective alone and in combination with standard-of-care temozolomide in an EGFRvIII-positive GBM xenograft model. Based on these results, ABBV-221 has advanced to a phase I clinical trial in patients with advanced solid tumors associated with elevated levels of EGFR. *Mol Cancer Ther; 17(4); 795–805. ©2018 AACR.*

Downloaded from http://aacrjournals.org/mct/article-pdf/17/4/795/1857864/795.pdf by guest on 18 March 2025

Introduction

The important role of the EGFR in tumor cell survival makes it an attractive therapeutic target, and both small molecules and antibodies directed against this receptor are approved for clinical use (1–3). Despite the success of these therapeutics, intrinsic and acquired resistance limits their effectiveness (4). In principle, EGFR-targeted antibody drug conjugates (ADC) that rely on target expression and not on inhibition of downstream signaling pathways for activity could circumvent some of these resistance mechanisms of current EGFR inhibitors and be more broadly active. Widespread normal tissue EGFR expression, however, represents a toxicity risk (5).

We have previously described depatux-m, a tumor-selective ADC comprised of the anti-EGFR antibody ABT-806 and the monomethyl auristatin F (MMAF) warhead (6). Depatux-m binds to a constitutively activated form of EGFR generated by deletion of exons 2 through 7 (EGFRde2–7 or EGFRvIII) and amplified or highly overexpressed wild-type EGFR (7). Depatux-m displays potent antitumor activity against xenograft models expressing these forms of EGFR (6). Depatux-m is currently being evaluated in glioblastoma multiforme (GBM) patients due to the high prevalence of EGFR amplification and EGFRvIII in this indication (8–10). Clinical responses have been observed in recurrent GBM including complete responses in EGFR-amplified patients, and evaluation of its potential benefit relative to standard of care is ongoing in multiple phase II/III trials in both front-line and recurrent GBM disease settings (11–13).

Although the incidence of EGFR amplification in solid tumors outside GBM is infrequent, EGFR overexpression, with levels of EGFR typically lower than seen in EGFR-amplified tumors, is common (14–16). In preclinical studies depatux-m was highly effective in xenograft models with ≥500,000 EGF receptors per cell, but when EGFR levels were lower the responses were variable (6). Consistent with these results, only a single partial response outside GBM was observed in a depatux-m phase I trial in patients with advanced solid tumors (17). The patient with the partial response had triple-negative breast cancer with EGFR amplification providing additional evidence that depatux-m may be

[1]AbbVie Inc., North Chicago, Illinois. [2]AbbVie Bioresearch Center, Worcester, Massachusetts. [3]Olivia Newton-John Cancer Research Institute, and La Trobe University Austin Hospital, Heidelberg, Victoria, Australia.

Note: Supplementary data for this article are available at Molecular Cancer Therapeutics Online (http://mct.aacrjournals.org/).

Current address for C.-M. Hsieh: Merck Research Laboratories, Boston, MA 02115.

Corresponding Author: Edward B. Reilly, AbbVie Inc., Oncology Discovery, R460, 1 North Waukegan Road, North Chicago, IL 60064. Phone: 847-937-0815; Fax: 847-938-1336; E-mail: ed.reilly@abbvie.com

doi: 10.1158/1535-7163.MCT-17-0710

©2018 American Association for Cancer Research.

Shanghai Miracogen Inc.- Ex. 2013, Page 000001
IPR2025-00685 (CSPC Megalith Biopharmaceutical Co., LTD. v. Shanghai Miracogen Inc.)

effective for tumors with this EGFR phenotype. These results indicate both an opportunity and unmet need to develop an EGFR therapeutic targeting tumors with moderate levels of EGFR overexpression.

The on-target toxicities of EGFR inhibitors, most notably characteristic skin toxicities, were not observed in the depatux-m clinical trials, consistent with low binding to normal tissue EGFR (11, 17). The dose-limiting toxicities in the depatux-m trials were reversible ocular side effects manifesting as blurred vision, corneal deposits, and foreign body sensation in the eye. The majority of the ocular-related adverse events were resolved or improved following administration of steroid eye drops or cessation of depatux-m treatment (11–13, 17). These toxicities have been observed with other MMAF conjugates, but typically are not seen with monomethyl auristatin E (MMAE)–based conjugates, suggesting a potential mitigation of this side effect with use of MMAE (18).

With the goal of developing a more broadly active EGFR-targeting therapeutic with reduced ocular side effects while retaining the tumor-selective properties of depatux-m, ABBV-221, an ADC comprised of an affinity-matured version of ABT-806 as the targeting antibody conjugated to a MMAE warhead, was generated. ABBV-221 is currently under clinical evaluation, and preclinical data supporting its development are described herein.

Materials and Methods

Antibodies and reagents

Recombinant forms of EGFR (soluble EGFR (sEGFR), wild-type extracellular domain (ECD); sEGFRde2-7 ECD; sEGFR^{C271A,C283A} ECD) were generated by AbbVie as previously described (7). Biotinylated EGFR was prepared using a sulfo-NHS-Biotin kit (Pierce Inc.) according to the manufacturer's protocol. Cetuximab (Bristol-Meyers Squibb) and temozolomide (TMZ; Merck & Co., Inc.) were purchased. ABT-806 was produced by transient transfection of HEK-293-6E cells as previously described (7). Maleimidocaproyl MMAF (mcMMAF) and valine–citrulline MMAE (vcMMAE) were provided by Seattle Genetics and conjugations and used to generate ADCs as previously described (19).

Cell culture

The tumor cell lines A431, NR6 fibroblasts, U87MG, and U87MGde2-7 (engineered to overexpress EGFRvIII) were obtained from the Ludwig Institute for Cancer Research (LICR; Melbourne, Australia; ref. 20). NCI-H292, HCT-15, NCI-1703, NCI-H441, LoVo, NCI-H292, FaDu, and SW620 cell lines were obtained from the ATCC. HCC827.ER.LMC was obtained from the ATCC and serially passaged by subcutaneous injection into mouse flank to improve growth characteristics. A431, NR6 fibroblast, NCI-H292, HCT-15, FaDu, NCI-H1703, and NCI-H441 cells were cultured in RPMI-1640 media supplemented with 10% FBS. SW620 and EBC1 cells were maintained in Leibovitz L15 media supplemented with 10% FBS. U87MG and U87MGde2-7 cells were maintained in DMEM media with high glucose, supplemented with 10% FBS and 1 mmol/L sodium pyruvate. U87MGde2-7 cells were maintained under selection with 400 μg/mL geneticin. LoVo cells were maintained in F-12K Nutrient Mixture supplemented with 10% FBS. Upon receipt, all cell lines were authenticated by short tandem repeat authentication and confirmed as mycoplasma-negative with the MycoAlert assay (Lonza Inc.). EGFR expression levels for cell lines not authenticated in the 6 months before use were confirmed by FACS analysis.

ABT-806 antibody affinity maturation

The affinity maturation of ABT-806 was performed using the Yeast Display Technology (21, 22). Sequence alignment analysis shows that the EGFR antibody ABT-806 shares the highest identity to human germlines IGHV4-4 and IGKV1-12. To improve the affinity of ABT-806 to EGFR, two sublibraries of ABT-806 were generated by PCR, using KOD Hot Start DNA Polymerase (Novagen). Limited mutagenesis was achieved by using primers having low degeneracy for the generation of diversity at key positions in heavy- and light-chain complementarity-determining regions (CDRs). The targeted positions in the heavy-chain library were: 30, 31, 32, 52, 53, 54, and the entire CDR3 (95 to 102). The targeted positions in the light-chain library were: 28, 30, 31, 32, 33, 50, 52, 53, 55, 56, 91, 92, and 93. Positions are according to the Kabat numbering scheme (23). The PCR product was cleaned and concentrated using MultiScreen-HTS PCR 96-well plates (Millipore) and used for electrotransformation of competent yeast cells of *Saccharomyces cerevisiae*. The library was grown on selective SD–UT media (dextrose-based media without ura and Trp; selection markers for pYDsTEV vector) overnight at 30°C. Library size was estimated from 10-fold serial dilutions and plating into SD–UT-based agar plates. A diversity of approximately 1×10^9 was achieved for both libraries.

Once libraries were established, four to six rounds of selection against decreasing concentrations of biotinylated EGFR were performed. Yeast cells expressing scFv ABT-806 antibody variants were allowed to bind for different times and temperatures before washing or addition of unlabeled EGFR competitor. All incubations and washes were in PBS containing 0.5% BSA. Bound biotinylated antigen was detected by flow cytometry analysis using commercially available fluorescence-labeled streptavidin. Selection for improved on-rate, off-rate, or overall affinity was carried out, and antibody protein sequences of affinity-modulated ABT-806 clones were recovered from yeast cells and reformatted from scFv to full-length IgG for further characterization.

Binding ELISA

Ninety-six well plates were coated with 1 μg/mL of mouse 6x-His epitope tag mAb (4A12E4; Life Technologies) at 4°C overnight and then blocked using 10% SuperBlock (Pierce) in PBS with 0.05% Tween 20 (PBS-T) for 2 hours at room temperature. Plates were washed 3 times with PBS-T and incubated with 100 μL of sEGFR ECD at 2 μg/mL for 1 hour at room temperature. Plates were washed 3 times with PBS-T, incubated with ABT-806 or depatux-m as appropriate at room temperature for 1 hour, washed 3 times with PBS-T, and incubated with 100 μL of goat anti-human IgG-HRP (Pierce) at room temperature for 1 hour. After washing plates 3 times in PBS-T, 100 μL of 3,3′,5,5′-tetramethylbenzidine (TMB; Pierce) were added to each well and incubated at room temperature until color developed (approximately 20 minutes). Reactions were stopped by addition of 100 μL 1 N phosphoric acid, and optical density was read at 450 nm.

FACS analysis

Cells were harvested from flasks when approximately 80% confluent using cell dissociation buffer (Life Technologies),

Downloaded from http://aacrjournals.org/mct/article-pdf/17/4/795/1857864/795.pdf by guest on 18 March 2025

Shanghai Miracogen Inc.- Ex. 2013, Page 000002

washed once in PBS/1% FBS (FACS buffer), and then resuspended at 2.5×10^6 cells/mL in FACS buffer. One hundred microliters of cells/well were added to a round-bottom 96-well plate. Ten microliters of a 10x concentration of mAb or ADC (final concentrations are indicated the figures) were added, and the plate was incubated at 4°C for 1 hour. For competition, FACS FITC-conjugated ABT-806 was added to a final concentration of 100 nmol/L, and then wells were washed twice in FACS buffer, suspended in 100 μL of PBS/1% formaldehyde, and analyzed on a Becton Dickinson LSRII flow cytometer. For standard FACS, cells were washed twice with FACS buffer and resuspended in 50 μL of Alexa Fluor 488 goat anti-human IgG secondary antibody conjugate (Life Technologies) diluted in FACS buffer. The plate was incubated at 4°C for 1 hour and washed twice with FACS buffer. Cells were resuspended in 100 μL of PBS/1% formaldehyde and analyzed on a LSRII flow cytometer. Data were analyzed using WinList flow cytometry analysis software.

Surface plasmon resonance of antibodies

A Biacore T100 surface plasmon resonance instrument (Biacore Life Sciences) was used to measure binding kinetics of recombinant soluble EGFR proteins forms (analytes) binding to anti-EGFR mAbs (ligands) as previously described (7).

Cytotoxicity assay

Cells were plated at 1,000 to 3,000 cells/well in complete growth medium containing 10% FBS in 96-well plates. The following day medium was removed and replaced with fresh media containing titrations of antibodies or ADCs, and cells were incubated for 72 hours at 37°C in a humidified CO_2 incubator. Cell viability was then assessed using an ATPlite luminescence assay (PerkinElmer) according to the manufacturer's instructions. A negative control ADC, rituximab-mcMMAF, was included in all assays to confirm that cell killing was antigen-dependent. Rituximab was selected as a negative control since this antibody binds to CD20, an antigen that is not expressed in any of the cell lines studied.

Determination of receptor density

EGFR density was determined by means of Quantum Simply Cellular (QSC) microspheres (Bangs Laboratories). Briefly, cells grown to 80% to 90% confluence were harvested using cell dissociation buffer (Life Technologies) or Versene (Life Technologies), transferred to 15 mL conical tubes, and combined with 6 mL FACS buffer [Ca^{2+}/Mg^{2+}-free Dulbecco's PBS (DPBS) + 1% FBS]. After centrifuging 5 minutes at 300 g, cells were resuspended in FACS buffer, counted, and then adjusted to a density of 2×10^6 cells/mL. One hundred microliters containing 2×10^5 cells were added to wells of a 96-well, round-bottom plate and incubated at 4°C with cetuximab (2 μg/mL) and rituximab (10 μg/mL) as positive and negative controls, respectively. Following 1-hour incubation with primary antibody, cells were centrifuged for 3 minutes at 300 × *g*, washed twice with FACS buffer, and then incubated for 1 hour at 4°C with Alexa Fluor 488 goat anti-human IgG (Life Technologies) diluted 1:100 in FACS buffer. Cells were then centrifuged for 3 minutes at 300 × *g*, washed twice with FACS buffer, and fixed with 100 μL/well of 1% formaldehyde in DPBS. The five standard bead populations from the QSC kit were prepared and stained with 1:100 Alexa Fluor 488 goat anti-human IgG (Life Technologies) according to the kit protocol. Bead standards resuspended in DPBS along with the fixed cell samples were then analyzed on a FACSCanto system (BD Biosciences). Data were interpreted via WinList software to generate geomean values. Geomean values for the bead populations were recorded in the provided lot-specific Quick Cal template, and a regression associating fluorescence geomean value to bead ABC value was calculated, resulting in a standard curve used to assign ABC (Antibody Binding Capacity or number of receptors) to stained cell samples.

Internalization and drug accumulation

To assess the internalization kinetics of ADCs, the amount of cellular free drug after treatment with ADCs was measured. A431, NCI-H292, and LoVo cells were grown in 6-well plates and treated with 15 μg/mL of depatux-m or ABBV-221. The treated cells were washed with PBS, detached from the plate, and centrifuged. The supernatant was aspirated, and the cells were frozen. A mixture of 95:5 acetonitrile and methanol with 50 nmol/L carbutamide internal standard was added to the cell pellets. The samples were vortexed, centrifuged, and transferred to 96-well plates containing 5% DMSO and 10% water. All samples were analyzed by liquid chromatography-tandem mass spectrometry using a Sciex 5500 triple quadrupole mass spectrometer alongside standard curves for quantitation of either free cys-mcMMAF or MMAE. Final drug concentrations were normalized to cell counts from each well.

In vivo studies

Female SCID, SCID-Beige, and nude mice were obtained from Charles River. Eight to 10 mice were housed per cage. The body weight upon arrival was 20 to 22 g. Food and water were available *ad libitum*. Mice were acclimated to the animal facilities for a period of at least 1 week prior to commencement of experiments. Animals were tested in the light phase of a 12-hour light:12-hour dark schedule (lights on at 06:00 hours). All experimental protocols were approved by and conducted in compliance with AbbVie's Institutional Animal Care and Use Committee and the National Institutes of Health Guide for Care and Use of Laboratory Animals Guidelines in a facility accredited by the Association for the Assessment and Accreditation of Laboratory Animal Care.

To generate xenografts, a suspension of viable tumors cells mixed with an equal amount of Matrigel (BD Biosciences) was injected subcutaneously into the flank of 6- to 8-week-old mice. The injection volume of 0.2 mL was composed of a 1:1 mixture of S-MEM and Matrigel (BD Biosciences). Tumors were size matched at approximately 200 to 250 mm^3. Therapy began the day of or 24 hours after size matching the tumors. Mice weighed approximately 25 g at the onset of therapy. Each experimental group included 8 to 10 animals. Tumors were measured 2 to 3 times weekly. Measurements of the length (L) and width (W) of the tumor were obtained via electronic calipers, and the volume was calculated according to the following equation: $V = L \times W^2/2$. Mice were euthanized when tumor volume reached a maximum of 3,000 mm^3 or upon presentation of skin ulcerations or other morbidities, whichever occurred first. For all groups, tumor volumes were plotted only until the full set of animals remained on study. If animals had to be taken off study, the remaining animals were monitored for tumor growth until they reached defined end-points.

Maximal tumor growth inhibition (TGI_{max}), expressed as a percentage, indicates the maximal divergence between the mean

Downloaded from http://aacrjournals.org/mct/article-pdf/17/4/795/1857864/795.pdf by guest on 18 March 2025

Shanghai Miracogen Inc.- Ex. 2013, Page 000003

tumor volume of the test article–treated group and the control group treated with drug vehicle or isotype-matched nonbinding human antibody (Ab 095) conjugated to either MMAE or MMAF. Tumor growth delay (TGD), expressed as a percentage, is the difference of the median time of the test article treated group tumors to reach 1 cm^3 as compared with the control group.

All experiments with the PDX GBM model were approved by and conducted in compliance with the Austin Health Animal Ethics Committee. Mice were inoculated with tumor subcutaneously and treatment commenced when tumors reached 60 mm^3. Treatments comprised an irrelevant ADC control (Ab 095), ABT-414, and ABBV-221 at 3 mg/kg every 4th day by intraperitoneal injection. Treatment commenced on day 35 after tumor inoculation and continued until day 78. Measurements of tumor growth were made as described above. Growth curves were generated until day 102 when mice from the control group had to be culled for ethical reasons. Other mice were followed up until they had to be culled for ethical reasons so as to allow for survival data to be collected for Kaplan–Meier curves, which were compared by the log-rank testing. Mice were censored for ill health, death, or euthanasia as per our institutional ethics guidelines. A human IgG1 ADC control to match the ABBV-221 isotype was included in all *in vivo* experiments.

SPECT imaging

Human tumor cells were implanted subcutaneously in the right flank of mice, and tumors were grown to approximately 250 mm^3 for imaging. Approximately 250 μCi of ^{111}In-labeled CHX-A"-DTPA conjugated ABT-806, AM1, or isotype control Ab was injected via tail vein in a volume of less than 200 μL (7). SPECT/CT imaging studies were performed to assess the *in vivo* tumor uptake of the radiolabeled mAb, and the animals were imaged at 4, 24, 48, 72, 120, and 168 hours after injection of radiolabeled mAb using a small animal nanoSPECT/CT (BioScan) equipped with four 9 pinhole 1.44 collimators. Anesthesia was induced using 2.0% isoflurane and air at a flow rate of 1.0 L/min. After induction, the anesthesia was maintained at 2% isoflurane/air. SPECT images were reconstructed using an Ordered-Subsets Expectation Maximization (OSEM) algorithm without attenuation or scatter correction, and CT data were reconstructed using a Filtered Back Projection with Shepp–Logan filtering algorithm. Images were coregistered, and regions of interest were drawn using Vivoquant image analysis software (inviCRO). The tumor uptake was quantified as a percentage of injected dose per cubic centimeter (%ID/cc).

Statistical analysis

IC_{50} and EC_{50} values were determined by nonlinear regression analysis of concentration response curves using GraphPad Prism 6.0. Data from *in vivo* experiments were analyzed using the two-way ANOVA with *post hoc* Bonferroni correction for TGI_{max}, and the Mantel–Cox log-rank test for TGD (GraphPad Prism, GraphPad Software).

Results

Affinity maturation of ABT-806 and generation of AM1

A yeast surface display affinity maturation protocol was used to generate a higher affinity ABT-806 variant that retained the unique tumor selectivity of the parental antibody. ABT-806 binds a cryptic epitope that is exposed by point mutations that disrupt a disulfide bridge ($EGFR^{C271A,C283A}$), allowing high affinity binding (7, 24). A recombinant form of this mutant $EGFR^{C271A,C283A}$ was used for initial selection of the library. Subsequent rounds of yeast-displayed library screening used a truncated form of the EGFR ECD ($EGFR^{1-501}$) that represents the untethered conformation of EGFR (24, 25). ABT-806 binds this form of the receptor with low affinity (7). A panel of EGFR variant antibodies was generated that bound recombinant $EGFR^{1-501}$ with up to several hundred-fold higher affinity than ABT-806 as measured by surface plasma resonance.

The affinity-matured variant AM1 was selected as the lead candidate based on binding properties intermediate between that of ABT-806 and cetuximab, as a higher affinity antibody similar to cetuximab may pose a significant toxicity risk as an ADC. AM1 has three amino acid differences in the heavy-chain CDRs and retains the intact parental ABT-806 light-chain sequence (Supplementary Fig. S1). AM1 binding to the untethered form of the receptor ($EGFR^{1-501}$) was increased 10-fold relative to ABT-806 (220 vs. 2,300 nmol/L); however despite this increased binding affinity, AM1 still binds with relatively low affinity to the untethered form of EGFR ($EGFR^{1-501}$) compared with cetuximab (220 vs. 4 nmol/L; Table 1). In contrast, although cetuximab binds to the untethered and full-length tethered form with similar high affinity, AM1 like the parental ABT-806 shows very weak binding to the full-length tethered form of EGFR (7). AM1, relative to ABT-806, shows a more modest improvement of binding to the EGFRvIII ECD (2.3 vs. 9.4 nmol/L; Table 1).

ABBV-221 binding and functional properties

ABBV-221 was generated by the conjugation of MMAE to the interchain disulfide bonds of AM1 via a valine–citrulline linker with an average drug-to-antibody ratio (DAR) of approximately 3 (26). To confirm that the binding characteristics of AM1 are retained in ABBV-221, ELISA-based binding assays were performed. AM1 and ABBV-221 show similar increased binding to $EGFR^{1-501}$ relative to depatux-m, although cetuximab binds with

Table 1. Affinity of ABT-806 and affinity-matured variants

	Surface plasmon resonance (binding constants)[a]							
	EGFR 1-501				EGFRvIII			
	k_a (1/Ms)	k_d (1/s)	K_D (M)	Fold increase[b]	k_a (1/Ms)	k_d (1/s)	K_D (M)	Fold increase[b]
Cetuximab	4.26E+05	1.71E−03	4.0E−09		3.46E+06	1.32E−03	3.8E−10	
ABT-806	3.53E+03	8.02E−03	2.3E−06		8.43E+04	7.93E−04	9.4E−09	
AM1	3.26E+03	7.31E−04	2.2E−07	10.1	7.61E+04	1.73E−04	2.3E−09	4.1

[a]EGFR: 6-point, 3-fold dilution series from 3 μmol/L to 12.35 nmol/L, fit to a 1:1 binding model using Biacore T100 Evaluation Software.
[b]The K_d ratio of the affinity-matured variant relative to the parental ABT-806 (AM variant K_d/ABT-806 K_d).

Downloaded from http://aacrjournals.org/mct/article-pdf/17/4/795/1857864/795.pdf by guest on 18 March 2025

Shanghai Miracogen Inc.- Ex. 2013, Page 000004

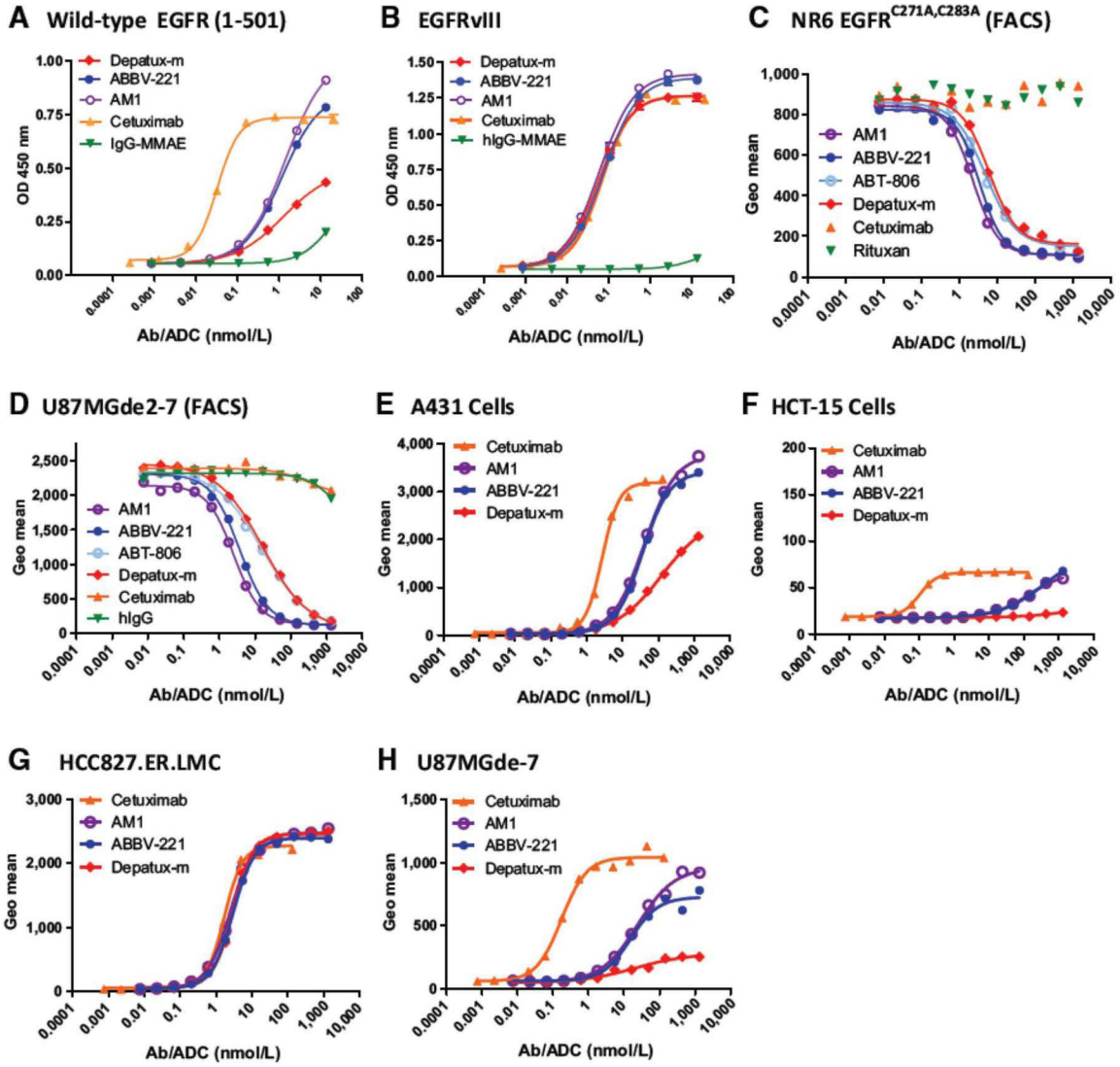


Figure 1.

ABBV-221 binding to soluble and cell surface expressed wild-type EGFR and EGFRvIII by ELISA and FACS. The ability of ABBV-221, AM1, depatux-m, ABT-806, cetuximab, and isotype control human IgG1 (huIgG1) to bind to $EGFR^{1-501}$ (**A**) and EGFRvIII (**B**) was assessed by ELISA. The ability of ABBV-221, AM1, depatux-m, ABT-806, cetuximab, and isotype control huIgG1 to compete with labeled ABT-806 for binding to NR6 $EGFR^{C271A,C283A}$ (**C**) and U87MGde2-7 (**D**) was assessed by competition-based FACS analysis. Direct binding of ABBV221, AM1, depatux-m, ABT-806, cetuximab, and isotype control huIgG1 to A431 (**E**), HCT-15 (**F**), HCC827.ER.LMC (**G**), and U87MGde2-7 (**H**) was assessed by FACS.

significantly increased apparent affinity (Fig. 1A). In contrast, depatux-m, ABBV-221, AM1, and cetuximab all display comparable binding to EGFRvIII (Fig. 1B).

To determine if AM1 and its conjugated derivative ABBV-221 bind to a similar tumor-selective EGFR epitope as does ABT-806/depatux-m, a competition-based FACS analysis was performed. Both AM1 and ABBV-221, unlike cetuximab, competed equally with fluorescein-conjugated ABT-806 for binding to cells engineered to express $EGFR^{C271A,C283A}$ or EGFRvIII (Fig. 1C and D). These results indicate that the affinity-matured AM1/ABBV-221 recognizes a similar tumor-selective epitope as ABT-806/depatux-m while displaying improved binding to wild-type EGFR; however, this binding is still significantly reduced compared with that of cetuximab. In contrast, binding of AM1/ABBV-221 and ABT-806/depatux-m to EGFRvIII is comparable.

Direct binding of AM1, ABBV-221, and depatux-m to tumor cell surface EGFR was also assessed by FACS analysis. Depatux-m binds to A431 tumor cells that overexpress wild-type EGFR, although even at high concentrations, this binding is not saturated (Fig. 1E). Relative to depatux-m, both AM1 and ABBV-221 bind with increased apparent affinity to these wild-type

Downloaded from http://aacrjournals.org/mct/article-pdf/17/4/795/1857864/795.pdf by guest on 18 March 2025

Shanghai Miracogen Inc.- Ex. 2013, Page 000005

Table 2. ABBV-221 cytotoxicity in human tumor cell lines

	Tumor type	EGFR genotype	Receptor number	Cytotoxicity (nmol/L)[a]
U87MGde2-7	Glioblastoma multiforme	EGFRvIII	1×10^6	0.2
A431	Vulvar epidermoid carcinoma	Wild-type	2×10^6	1
HCC827.ER.LMC	Lung adenocarcinoma	Wild-type, E746_A750	5.85×10^5	11
EBC1	Lung squamous cell carcinoma	Wild-type	1.84×10^5	69
NCI-H1703	Lung squamous cell carcinoma	Wild-type	2.8×10^5	4
NCI-H441	Lung adenocarcinoma	Wild-type	1.4×10^5	80
NCI-H292	Lung adenocarcinoma	Wild-type	ND[b]	60
FaDu	Squamous cell carcinoma of the hypopharynx	Wild-type	4.77×10^5	8
LoVo	Colorectal adenocarcinoma	Wild-type	1.28×10^5	8
HCT15	Colorectal adenocarcinoma	Wild-type	0.95×10^5	>1,000
SW620	Colorectal adenocarcinoma	EGFR-null	-	>1,000

[a] Cell viability was determined following incubation with ABBV-221 for 72 hours. The values represent IC_{50s}. Unconjugated AM1 does not inhibit growth of any of these cell lines.
[b] ND, not determined—an accurate number could not be obtained due to clumping of cells.

EGFR-expressing cells, although binding affinity is still significantly lower than that observed with cetuximab (Fig. 1E). Evaluation of the binding to HCT-15 cells with lower levels of wild-type EGFR expression shows a similar pattern of binding, although the binding is reduced compared with A431 cells (Fig. 1F). This result is consistent with an avidity effect contributing to elevated ABBV-221 binding to cells with high levels of EGFR, as increased antigen density will increase the probability of more stable bivalent binding of two EGF receptors. ABBV-221 also binds to HCC827.ER.LMC tumor cells (Fig. 1G). The HCC827.ER.LMC tumor cell line contains an EGFR-activating exon 19 deletion of EGFR found in a subset of non–small cell lung cancer (NSCLC) lines (6). Consistent with results from the ELISA assay, depatux-m, ABBV-221, AM1, and cetuximab all display comparable binding to EGFRvlll-expressing GBM cells (Fig. 1H).

ABBV-221 *in vitro* cytotoxicity against EGFR-expressing cells

The cytotoxic activity of ABBV-221 across a panel of a tumor cell lines overexpressing wild-type or mutant forms of EGFR was evaluated in cell killing assays. The most sensitive cell lines were inhibited by single-digit nanomolar concentrations of ABBV-221, and, similar to depatux-m, increased activity was observed in the cell lines with higher levels of EGFR (Table 2).

ABBV-221 and ABT-414 *in vitro* and *in vivo* tumor uptake

In order to determine if the increased affinity of the targeting antibody in ABBV-221 relative to depatux-m would increase tumor uptake, intracellular accumulation of the released warhead (MMAE or cys-MMAF) following treatment of tumor cells was measured. In each of the cell lines (A431, H292, and LoVo) assessed, ABBV-221–treated cells had a higher intracellular warhead concentration relative to depatux-m–treated cells (Fig. 2A–C). In addition, intracellular warhead concentration is highest in the cells with high EGFR receptor expression.

To assess the impact of increased affinity of AM1 relative to ABT-806 on tumor uptake *in vivo*, mice bearing xenografts were injected with [^{111}In]ABT-806, [^{111}In]AM1, or [^{111}In]hIgG1 and imaged over a 120-hour time course. The %ID/cc was plotted against time for three xenograft models A431, H292, and EBC1 (Fig. 2D–F). In each of the models, AM1 displayed an increased tumor uptake relative to ABT-806 consistent with the hypothesis that the increased affinity of the antibody results in greater tumor uptake.

ABBV-221 *in vivo* efficacy in EGFR-expressing xenograft tumor models

Although the frequency of EGFR amplification is low in NSCLC (5%–7%), EGFR overexpression is common. The efficacy of ABBV-221 compared with that of depatux-m was evaluated in several nonamplified wild-type EGFR-positive NSCLC xenograft models. ABBV-221 induced sustained tumor regressions in NCI-H1703, H292, and EBC xenografts after administration of between 1 and 6 mg/kg dosed every 4 days for a total of six doses (Fig. 3A–C). These models expressed a range of EGFR levels as assessed using immunohistochemistry, although all have lower levels of EGFR than observed in amplified models. No obvious correlation between EGFR expression level and response was observed, although all were sensitive to ABBV-221–mediated killing. Multiple factors can influence ADC activity beyond receptor density including efficiency of ADC internalization and vascularity of tumors. In all the models, the antitumor effect of ABBV-221 was superior to depatux-m when dosed equivalently.

Comparison of ABT-806 and AM1 MMAE versus MMAF conjugates

In principle, improved activity of ABBV-221 relative to depatux-m in these NSCLC models could be due to either the higher affinity of the targeting antibody, the distinct warheads, or a combination of both. To determine the contribution of antibody and warhead to improved activity of ABBV-221, both ABT-806 and AM1 MMAE and MMAF conjugates were generated and assessed for antitumor activity in a fourth NSCLC xenograft model (NCI-H441). ABT-806 MMAE and ABT-806 MMAF (depatux-m) dosed at 3 mg/kg had similar antitumor activity (Fig. 3D). Similarly, AM1 MMAE (ABBV-221) and AM1 MMAF also had comparable antitumor activity, although, consistent with the other NSCLC models, the AM1-based conjugates were significantly more potent than the ABT-806 conjugates resulting in tumor regressions (Fig. 3D). These results suggest that the improved efficacy of ABBV-221 relative to depatux-m is driven primarily by the increased affinity of the antibody and not the distinct warhead.

ABBV-221 activity in an EGFRvIII-expressing GBM model

Depatux-m binds EGFRvIII with high affinity and has significant antitumor activity alone and in combination with SOC TMZ and radiation in the U87MGde2-7 GBM model that expresses EGFRvIII (6). This model was used to compare the

Downloaded from http://aacrjournals.org/mct/article-pdf/17/4/795/1857864/795.pdf by guest on 18 March 2025

Shanghai Miracogen Inc.- Ex. 2013, Page 000006

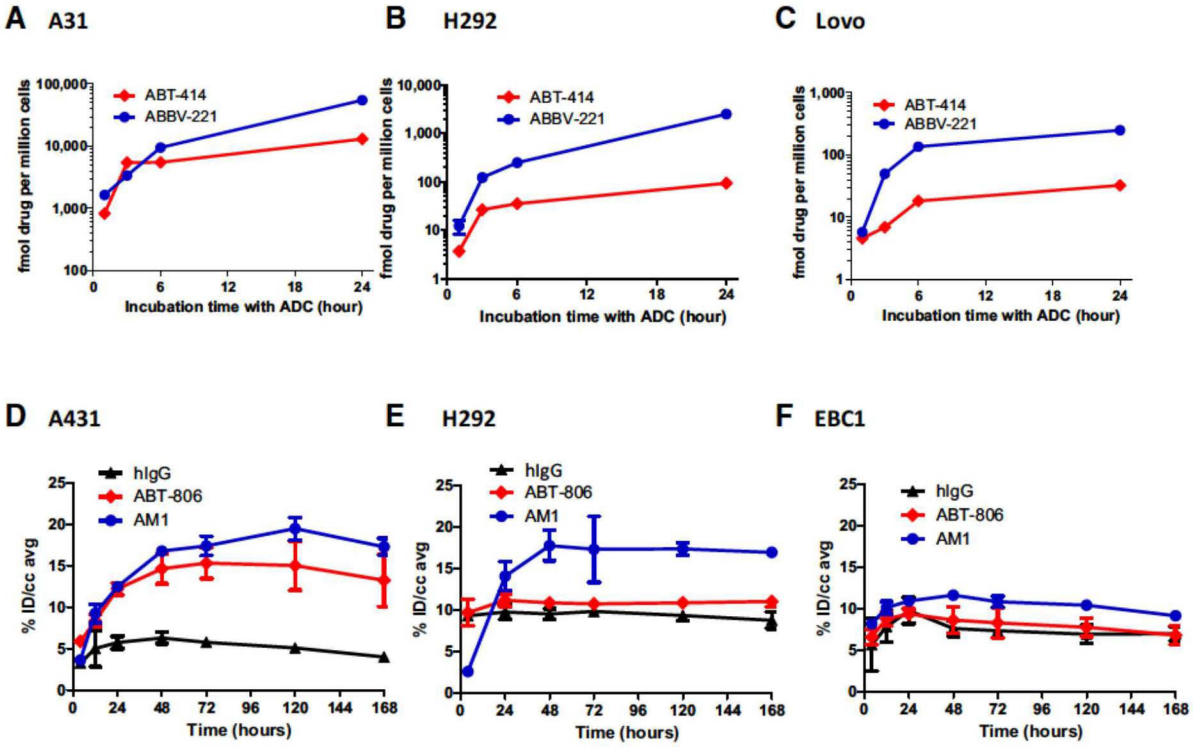


Figure 2.

ABBV-221 and ABT-414 tumor uptake (*in vitro* and *in vivo*). The intracellular accumulation of MMAE or cys-MMAF was measured following ABBV-221 or ABT-414 incubation with A431 (**A**), H292 (**B**), and LoVo (**C**) cell lines. The percentage tumor uptake (%ID/cc) of ^{111}Indium-labeled ABT-806, AM1, or negative control human igG1 was measured by SPECT imaging in A431 (**D**), H292 (**E**), and EBC1 (**F**) xenograft tumors.

activities of depatux-m and ABBV-221 alone and in combination with standard of care. Suboptimal doses of ADCs were combined with TMZ and radiation to permit assessment of the triple combination. Consistent with previous results demonstrating that low doses of depatux-m had modest activity as monotherapy, low dose ABBV-221 (1 mg/kg, Q4D x 6) also had minimal activity (Fig. 4A; ref. 6). In combination with TMZ and radiation, however, ABBV-221, similar to the triple combination with depatux-m, was highly effective in inducing sustained regressions and complete responses in this model (Fig. 4B). AM1 MMAF was also evaluated in parallel in these experiments as monotherapy and as a triple combination. AM1 MMAF displayed similar combination activity as ABBV-221 and a modestly improved single-agent activity (Fig. 4A and B).

To further assess the potential of ABBV-221 in GBM, an EGFR-amplified PDX model was evaluated. In this GBM model, ABBV-221 and depatux-m treatment resulted in similar antitumor activity (Fig. 4C).

Discussion

ABBV-221 is a re-engineered EGFR-targeting ADC designed to retain the tumor-selective properties of depatux-m. The increased affinity of ABBV-221 relative to depatux-m may expand its utility beyond EGFR-amplified tumors to those with EGFR overexpression. The key to the tumor selectivity of depatux-m resides in the cryptic epitope on EGFR which is accessible primarily in tumors when EGFR is in the untethered "extended" conformation (24). Several observations suggest that this tumor selectivity is retained by ABBV-221. First, AM1 was selected as the parent antibody for ABBV-221 from a panel of ABT-806 affinity-matured variants based on its increased affinity for wild-type EGFR. Despite approximately 10-fold higher affinity relative to depatux-m, ABBV-221 still binds the $EGFR^{1-501}$ untethered, "extended" form of the receptor ($EGFR^{1-501}$) with relatively low affinity compared with cetuximab. This was a critical selection criterion as cetuximab-like antibodies have limited potential as ADCs because of significant binding to normal tissues. Second, although both depatux-m and ABBV-221 bind recombinant untethered EGFR, neither antibody displays significant binding to recombinant wild-type EGFR in the tethered conformation. Third, ABBV-221 competes with depatux-m for binding to cells expressing $EGFR^{C271A,C283A}$ or EGFRvIII suggesting binding to the same or overlapping epitope. It is therefore likely that tumor-selective binding will be preserved in ABBV-221 despite the higher affinity binding for wild-type EGFR, and this is further supported by a low frequency of skin rash observed in the ABBV-221 phase I trial (27).

ABBV-221 was developed with the goal of extending activity to tumors that exhibit EGFR overexpression, but have lower levels of protein than EGFR-amplified tumors. The antitumor activity of ABBV-221 was evaluated in four NSCLC models as this tumor type has significant unmet need and EGFR overexpression is common. These four models expressed a range of

Downloaded from http://aacrjournals.org/mct/article-pdf/17/4/795/1857864/795.pdf by guest on 18 March 2025

Shanghai Miracogen Inc.- Ex. 2013, Page 000007

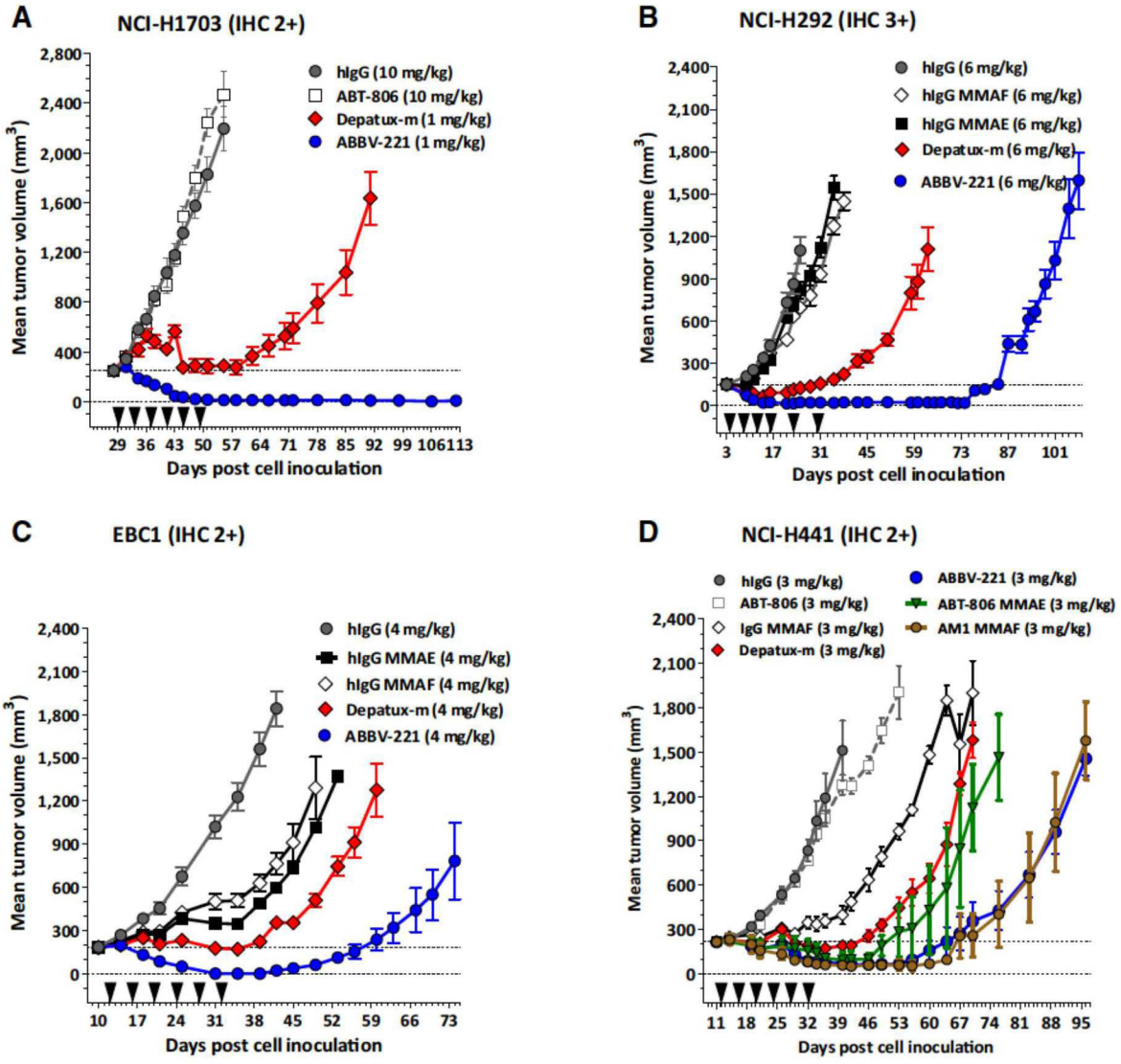


Figure 3.

Efficacy of EGFR ADCs in lung xenograft tumor models. The *in vivo* potency of ABBV-221 was compared with depatux-m in mice implanted with NCI-H1703 (**A**), NCI-H292 (**B**), EBC1 (**C**), and NCI-H441 (**D**) tumor xenografts. The ADCs or antibodies were administered at doses indicated in the figure on a Q4Dx6 schedule.

EGFR and scored as 2+ or 3+ as assessed by IHC. The IHC assay utilized here is the same assay used clinically with an H-scoring paradigm to retrospectively classify tumors as high and low EGFR in the FLEX NSCLC trial evaluating the activity of cetuximab in combination with chemotherapy (28). Although our scoring method is simpler, all four of the models would fall within the high category as defined in this retrospective analysis (28). The antitumor activity and increased potency of ABBV-221 relative to depatux-m suggests that this may be a relevant patient population for ABBV-221.

Direct comparison of AM1-based ADCs generated with either MMAE or MMAF in a NSCLC model indicates the potency of MMAE and MMAF conjugates is similar, suggesting the increased affinity of ABBV-221 underlies its improved antitumor activity. Although this conclusion is based on a single tumor model, it is consistent with previous findings comparing ABT-806 MMAE and ABT-806 MMAF (depatux-m) conjugates across ten xenograft models where only modest differences in activity were observed (6). In addition, ABBV-221 treatment drives increased intracellular warhead accumulation relative to depatux-m, and [^{111}In]AM1 displays elevated tumor uptake relative to [^{111}In]ABT-806 (Fig. 2), suggesting that the increased affinity of AM1 is a key determinant of elevated activity of ABBV-221.

Objective responses including complete responses have been observed for depatux-m in EGFR-amplified GBM patients as

Downloaded from http://aacrjournals.org/mct/article-pdf/17/4/795/1857864/795.pdf by guest on 18 March 2025

Shanghai Miracogen Inc.- Ex. 2013, Page 000008

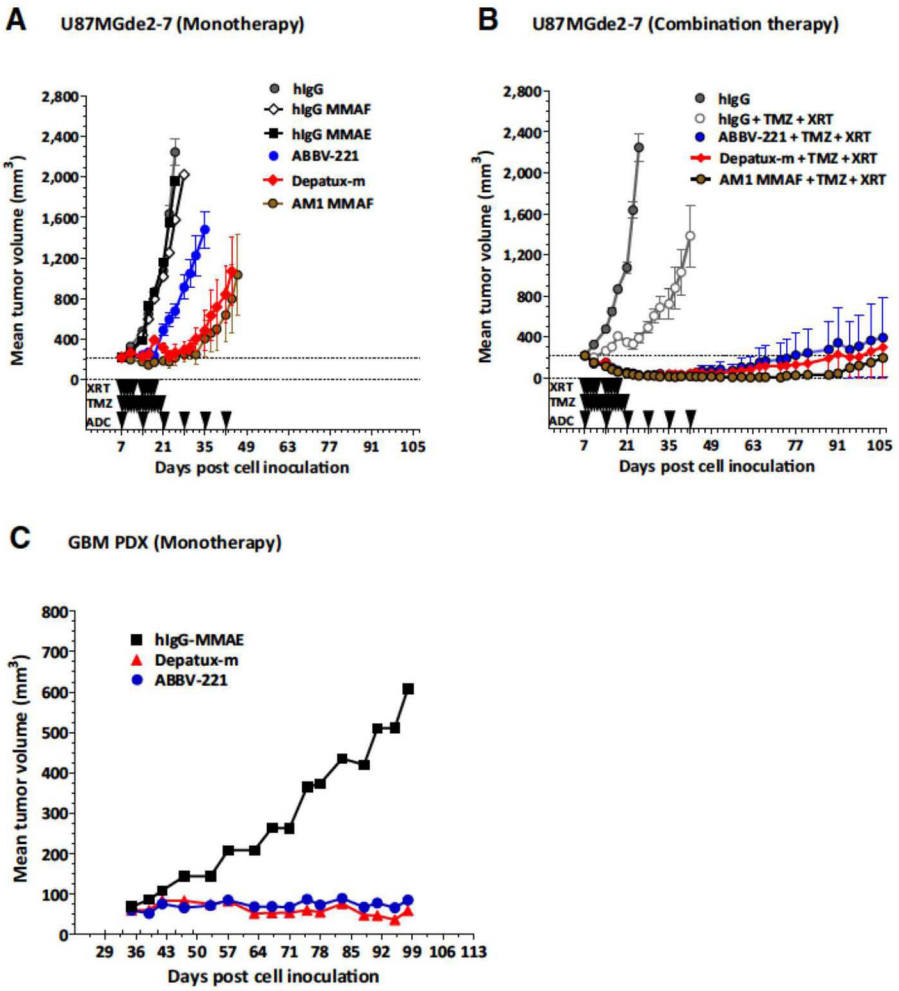


Figure 4.
ABBV-221 monotherapy and combination therapy with TMZ and fractionated radiation in a GBM xenograft model. The *in vivo* potency of ABBV-221 was compared with depatux-m and AM1 MMAF as monotherapy (**A**) and as triple combination with TMZ and fractionated radiation (XRT) in the U87MGde2–7 xenograft model (**B**). ADCs and antibodies were dosed at 1 mg/kg, TMZ at 1.5 mg/kg, and XRT at 2 Gy at the times indicated by the arrows. hIgG indicates an isotype control nontargeting negative control human IgG. The *in vivo* potency of ABBV-221 was compared with depatux-m in an EGFR-amplified PDX GBM model (**C**). ADCs were dosed at 3 mg/kg Q4Dx6.

both monotherapy and in combination with SOC (11–13, 17). The EGFRvIII mutation is prevalent in GBM occurring almost exclusively within the EGFR-amplified patient population. Depatux-m and ABBV-221, as part of a triple combination regimen with TMZ and radiation, had similar efficacy in the U87MGde2-7 GBM model expressing high levels of EGFRvIII. Because depatux-m already has high affinity for EGFRvIII, it is not surprising the small affinity improvement for ABBV-221 does not translate into improved antitumor activity against cells overexpressing this mutant form of the EGF receptor. ABBV-221 also has similar activity as depatux-m against an EGFR-amplified GBM PDX model, suggesting that ABBV-221 may have activity similar to depatux-m in this patient population with the potential to extend potency to patients with EGFR-nonamplified, overexpressed GBM. Novel treatments for GBM are urgently needed (29–31). Ultimately, it will be interesting to evaluate the activity of ABBV-221 in a series of wild-type EGFR-amplified and -nonamplified, overexpressed GBM tumor models to determine if they show an enhanced sensitivity relative to depatux-m.

The switch of the linker drug from mcMMAF for depatux-m to vcMMAE for ABBV-221 was motivated in part to circumvent the corneal side effects observed with depatux-m. This side effect appears to be a class effect of certain microtubulin-inhibiting ADC warheads and has been observed with other MMAF- and DM4-based ADCs (18). Corneal side effects are not typically observed with MMAE-based ADCs so switching to the MMAE warhead in ABBV-221 may mitigate its occurrence. In support of this hypothesis, corneal effects (including clinical, ophthalmologic, and microscopic findings in the corneal epithelium) were observed in nonhuman primates treated with depatux-m but were less severe with ABBV-221 suggesting reduced risk of corneal side effects as compared with depatux-m. The primary nonclinical toxicities associated with ABT-221 included effects on the epithelium of various tissues (including skin) and bone marrow. Furthermore, early clinical data with ABBV-221 strongly support a reduced risk of corneal toxicity where to date the main toxicities observed have been infusion reactions (27). Dosing of ABBV-221 has cleared 10 cohorts (42 patients) at doses up to 4.5 mg/kg on a 3-week cycle, and only a single case of keratitis has been observed, contrasting with the prevalent corneal toxicity profile of depatux-m (27).

The reduced risk for corneal side effects and increased antitumor activity of ABBV-221 suggest it may be an attractive

Downloaded from http://aacrjournals.org/mct/article-pdf/17/4/795/1857864/795.pdf by guest on 18 March 2025

Shanghai Miracogen Inc.- Ex. 2013, Page 000009

therapeutic candidate for cancers such as NSCLC and various squamous carcinomas where EGFR overexpression is frequent, but amplification is rare. In addition, ABBV-221 may have utility in GBM targeting both EGFR-amplified patients and the potential to extend activity to patients with nonamplified EGFR overexpression. Based on the preclinical data described here, ABBV-221 has advanced to a phase I trial in patients with tumors likely to overexpress EGFR.

Disclosure of Potential Conflicts of Interest

A.C. Phillips has ownership interest (including patents) in AbbVie. P.J. DeVries is Research Scientist at, and has ownership interest (including patents) in, AbbVie. C.-M. Hsieh has ownership interest (including patents) in US Patent. H.K. Gan reports receiving commercial research grant from AbbVie. A.M. Scott is Consultant at Life Science Pharmaceuticals, reports receiving commercial research grant from AbbVie, reports receiving other commercial research support from EMD Serono, and has ownership interest (including patents) in Ludwig Institute for Cancer Research. No potential conflicts of interest were disclosed by the other authors.

Authors' Contributions

Conception and design: A.C. Phillips, E.R. Boghaert, K.S. Vaidya, C.-M. Hsieh, F.G. Buchanan, S.R. Mudd, E.B. Reilly

Development of methodology: A.C. Phillips, H.D. Falls, P.J. DeVries, L. Benatuil, C.-M. Hsieh, J.A. Meulbroek, M.J. Voorbach, S.R. Mudd, E.B. Reilly

Acquisition of data (provided animals, acquired and managed patients, provided facilities, etc.): E.R. Boghaert, K.S. Vaidya, H.D. Falls, M.J. Mitten, P.J. DeVries, L. Benatuil, J.A. Meulbroek, S.C. Panchal, K.R. Durbin, M.J. Voorbach, D.R. Reuter, L.I. Loberg, H.K. Gan, A.M. Scott

Analysis and interpretation of data (e.g., statistical analysis, biostatistics, computational analysis): A.C. Phillips, E.R. Boghaert, K.S. Vaidya, H.D. Falls, P.J. DeVries, J.A. Meulbroek, S.C. Panchal, F.G. Buchanan, K.R. Durbin, M.J. Voorbach, D.R. Reuter, S.R. Mudd, L.I. Loberg, H.K. Gan, A.M. Scott, E.B. Reilly

Writing, review, and/or revision of the manuscript: A.C. Phillips, E.R. Boghaert, K.S. Vaidya, H.D. Falls, M.J. Mitten, P.J. DeVries, L. Benatuil, J.A. Meulbroek, S.C. Panchal, F.G. Buchanan, M.J. Voorbach, D.R. Reuter, S.R. Mudd, L.I. Loberg, S.L. Ralston, H.K. Gan, A.M. Scott, E.B. Reilly

Administrative, technical, or material support (i.e., reporting or organizing data, constructing databases): M.J. Mitten, D.R. Reuter, S.R. Mudd, E.B. Reilly

Study supervision: A.C. Phillips, E.R. Boghaert, K.S. Vaidya, C.-M. Hsieh, S.R. Mudd, L.I. Loberg, E.B. Reilly

Acknowledgments

The design, conduct, and financial support for the study were provided by AbbVie.

The costs of publication of this article were defrayed in part by the payment of page charges. This article must therefore be hereby marked *advertisement* in accordance with 18 U.S.C. Section 1734 solely to indicate this fact.

Received July 31, 2017; revised December 7, 2017; accepted February 6, 2018; published first February 26, 2018.

References

1. Mendelsohn J, Baselga J. Epidermal growth factor receptor targeting in cancer. Semin Oncol 2006;33:369 85.
2. Enrique AA, Gema PC, Jeronimo JC, Auxiliadora GE. Role of anti-EGFR target therapy in colorectal carcinoma. Front Biosci (Elite Ed) 2012; 4:12 22.
3. Landi L, Cappuzzo F. EGFR TKIs as maintenance therapy in NSCLC: finding the old in the new INFORMation. Translat Lung Cancer Res 2012;1:160 2.
4. Chong CR, Janne PA. The quest to overcome resistance to EGFR-targeted therapies in cancer. Nat Med 2013;19:1389 400.
5. Li T, Perez-Soler R. Skin toxicities associated with epidermal growth factor receptor inhibitors. Target Oncol 2009;4:107 19.
6. Phillips AC, Boghaert ER, Vaidya KS, Mitten MJ, Norvell S, Falls HD, et al. ABT-414, an antibody-drug conjugate targeting a tumor-selective EGFR epitope. Mol Cancer Ther 2016;15:661 9.
7. Reilly EB, Phillips AC, Buchanan FG, Kingsbury G, Zhang Y, Meulbroek JA, et al. Characterization of ABT-806, a humanized tumor-specific anti-EGFR monoclonal antibody. Mol Cancer Ther 2015;14:1141 51.
8. Crespo I, Vital AL, Gonzalez-Tablas M, Patino Mdel C, Otero A, Lopes MC, et al. Molecular and genomic alterations in glioblastoma multiforme. Am J Pathol 2015;185:1820 33.
9. Hatanpaa KJ, Burma S, Zhao D, Habib AA. Epidermal growth factor receptor in glioma: signal transduction, neuropathology, imaging, and radioresistance. Neoplasia 2010;12:675 84.
10. Hill C, Hunter SB, Brat DJ. Genetic markers in glioblastoma: prognostic significance and future therapeutic implications. Adv Anat Pathol 2003; 10:212 7.
11. Gan HK, Fichtel L, Lassman AB, Merrell R, Van Den Bent MJ, Kumthekar P, et al. A phase 1 study evaluating ABT-414 in combination with temozolomide (TMZ) for subjects with recurrent or unresectable glioblastoma (GBM). J Clin Oncol 2014;35:2021.
12. Reardon DA, Lassman AB, van den Bent M, Kumthekar P, Merrell R, Scott AM, et al. Efficacy and safety results of ABT-414 in combination with radiation and temozolomide in newly diagnosed glioblastoma. Neuro-oncol 2017;19:965 75.
13. Gan HK, Reardon DA, Lassman AB, Merrell R, van den Bent M, Butowski N, et al. Safety, pharmacokinetics and antitumor response of depatuxizumab mafodotin as monotherapy or in combination with temozolomide in patients with glioblastoma. Neuro-oncol 2017 Oct 25. [Epub ahead of print].
14. Cancer Genome Atlas Network. Comprehensive genomic characterization defines human glioblastoma genes and core pathways. Nature 2008;455: 1061 8.
15. Cancer Genome Atlas Network. Comprehensive genomic characterization of squamous cell lung cancers. Nature 2012;489:519 25.
16. Cancer Genome Atlas Network. Comprehensive genomic characterization of head and neck squamous cell carcinomas. Nature 2015;517: 576 82.
17. Goss GD, Vokes EE, Gordon MS, Gandhi L, Papadopoulos KP, Rasco DW, et al. ABT-414 in patients with advanced solid tumors likely to overexpress the epidermal growth factor receptor (EGFR). J Clin Oncol 2015;33:2510.
18. Eaton JS, Miller PE, Mannis MJ, Murphy CJ. Ocular adverse events associated with antibody-drug conjugates in human clinical trials. J Ocul Pharmacol Ther 2015;31:589 604.
19. Doronina SO, Mendelsohn BA, Bovee TD, Cerveny CG, Alley SC, Meyer DL, et al. Enhanced activity of monomethylauristatin F through monoclonal antibody delivery: effects of linker technology on efficacy and toxicity. Bioconjug Chem 2006;17:114 24.
20. Mishima K, Johns TG, Luwor RB, Scott AM, Stockert E, Jungbluth AA, et al. Growth suppression of intracranial xenografted glioblastomas overexpressing mutant epidermal growth factor receptors by systemic administration of monoclonal antibody (mAb) 806, a novel monoclonal antibody directed to the receptor. Cancer Res 2001;61: 5349 54.
21. Feldhaus MJ, Siegel RW. Yeast display of antibody fragments: a discovery and characterization platform. J Immunol Methods 2004;290:69 80.
22. Cherf GM, Cochran JR. Applications of yeast surface display for protein engineering. Methods Mol Biol 2015;1319:155 75.
23. Kabat EA, Wu TT. Identical V region amino acid sequences and segments of sequences in antibodies of different specificities. Relative contributions of VH and VL genes, minigenes, and complementarity-determining regions to binding of antibody-combining sites. J Immunol 1991; 147:1709 19.

Downloaded from http://aacrjournals.org/mct/article-pdf/17/4/795/1857864/795.pdf by guest on 18 March 2025

Shanghai Miracogen Inc.- Ex. 2013, Page 000010

24. Garrett TP, Burgess AW, Gan HK, Luwor RB, Cartwright G, Walker F, et al. Antibodies specifically targeting a locally misfolded region of tumor associated EGFR. Proc Natl Acad Sci U S A 2009;106:5082 7.
25. Burgess AW, Cho HS, Eigenbrot C, Ferguson KM, Garrett TP, Leahy DJ, et al. An open-and-shut case? Recent insights into the activation of EGF/ErbB receptors. Mol Cell 2003;12:541 52.
26. Doronina SO, Toki BE, Torgov MY, Mendelsohn BA, Cerveny CG, Chace DF, et al. Development of potent monoclonal antibody auristatin conjugates for cancer therapy. Nat Biotechnol 2003;21:778 84.
27. Calvo E, Cleary JM, Moreno V, Gifford M, Roberts-Rapp L, Ansell PJ, et al. Preliminary results from a phase 1 study of the antibody-drug conjugate ABBV-221 in patients with solid tumors likely to express EGFR. J Clin Oncol 2017;35:15s, (suppl; abstr 2510).
28. Douillard JY, Pirker R, O'Byrne KJ, Kerr KM, Storkel S, von Heydebreck A, et al. Relationship between EGFR expression, EGFR mutation status, and the efficacy of chemotherapy plus cetuximab in FLEX study patients with advanced non-small-cell lung cancer. J Thorac Oncol 2014;9:717 24.
29. Johnson DR, Galanis E. Medical management of high-grade astrocytoma: current and emerging therapies. Semin Oncol 2014;41: 511 22.
30. Henson JW. Treatment of glioblastoma multiforme: a new standard. Arch Neurol 2006;63:337 41.
31. Blumenthal DT, Schulman SF. Survival outcomes in glioblastoma multiforme, including the impact of adjuvant chemotherapy. Expert Rev Neurother 2005;5:683 90.

Downloaded from http://aacrjournals.org/mct/article-pdf/17/4/795/1857864/795.pdf by guest on 18 March 2025

Shanghai Miracogen Inc.- Ex. 2013, Page 000011